

Spin-Valleytronics in Silicene: Quantum-Spin-Quantum-Anomalous Hall Insulators and Single-Valley Semimetals

Motohiko Ezawa

Department of Applied Physics, University of Tokyo, Hongo 7-3-1, 113-8656, Japan

Valley-based electronics, known as valleytronics, is one of the keys to break through to a new stage of electronics. The valley degree of freedom is ubiquitous in the honeycomb lattice system. The honeycomb lattice structure of silicon called silicene is an fascinating playground of valleytronics. We investigate topological phases of silicene by introducing different exchange fields on the A and B sites. There emerges a rich variety of topologically protected states each of which has a characteristic spin-valley structure. The single Dirac-cone semimetal is such a state that one gap is closed while the other three gaps are open, evading the Nielsen-Ninomiya fermion-doubling problem. We have newly discovered a hybrid topological insulator named the quantum-spin-quantum-anomalous Hall insulator, where the quantum anomalous Hall effect occurs at one valley and the quantum spin Hall effect occurs at the other valley. Along its phase boundary, single-valley semimetals emerge, where only one of the two valleys is gapless with degenerated spins. These semimetals are also topologically protected because they appear in the interface of different topological insulators. Such a spin-valley dependent physics will be observed by optical absorption or edge modes.

I. INTRODUCTION

The intrinsic degrees of freedom of an electron are its charge and spin, which lead to electronics and spintronics. The valley degree of freedom on honeycomb lattices is expected to provide us with the notion of valleytronics. Valleytronics was originally proposed in graphene¹⁻³, where the states near the Fermi energy are π orbitals residing near the K and K' points at opposite corners of the hexagonal Brillouin zone. The low-energy dynamics in the K and K' valleys is described by the Dirac theory. The valley excitations are protected by the suppression of intervalley scattering. However it is hard to realize valleytronics in graphene since the gap is closed and since it is difficult to discriminate between the K and K' points experimentally. In this context, transition metal dichalcogenides⁴⁻⁷ become a new playground of valleytronics, where a considerably large gap is open. In the most recent experimental progress, the identity of valleys manifests as valley-selective circular dichroism, leading to valley polarization with circularly polarized light, offering a possibility to a realization of valleytronics³⁻⁷.

Recently, another honeycomb system of silicon named silicene has been experimentally synthesized⁸⁻¹⁰ and theoretically explored¹¹⁻¹⁴. As prominent properties, it consists of buckled sublattices made of A sites and B sites, and the Dirac electron has a mass. The buckled structure allows us to control the Dirac mass independently at the K and K' points by applying external fields such that electric field¹², exchange field¹³ and photo-irradiation¹⁴. It is possible to generate a rich variety of topologically protected states in silicene, each of which has a characteristic spin-valley structure.

In this paper we propose to make a full control of the Dirac mass in order to search for new topological states together with new spin-valley structures in silicene. The Dirac mass can be fully controlled by four potential terms corresponding to the spin and valley degrees of freedom, among which three terms have already been studied¹²⁻¹⁴. The last one is driven by applying the staggered exchange field $\Delta M \equiv M_A - M_B$,

where M_A and M_B are exchange fields operating on the A and B sites, respectively. These four terms move Dirac cones, respecting the electron-hole symmetry. It is also possible to introduce four other potential terms, which shift Dirac cones so as to break the electron-hole symmetry. The typical one is driven by applying the mean staggered exchange field $\overline{M} \equiv \frac{1}{2}(M_A + M_B)$.

Well-known topologically protected states are quantum spin Hall (QSH) insulator¹⁵ and quantum anomalous Hall (QAH) insulator¹⁶⁻²¹. They are characterized by the helical and chiral gapless edge modes, respectively, according to the bulk-edge correspondence²²⁻²⁴. The QAH effect is the quantum Hall effect without Landau levels, while the QSH effect is the quantum Hall effect of spins rather than charges.

By introducing the staggered exchange field ΔM , we obtain rich phase diagrams as illustrated in Fig.1 and Fig.3. First of all, we are able to generate the spin-polarized QAH (SQAH) insulator together with single Dirac-cone (SDC) semimetals along its phase boundaries [Fig.2]. The SDC semimetal is a remarkable state that has one massless Dirac cone and three massive Dirac cones, evading the Nielsen-Ninomiya fermion-doubling problem²⁵. Second, a new finding is the quantum-spin-quantum-anomalous Hall (QSQA) insulator. It is a new type of topological insulator such that, e.g., the QAH effect is realized at the K point while the QSH effect is realized at the K' point [Fig.4]. Third, another new finding is a single-valley (SV) semimetal such that, e.g., the gap is open (closed) at the K (K') point with spin degeneracy. It is different from the SDC state which has only one closed gap without spin degeneracy. These spin-valley dependent band structures will be experimentally observed by spin-valley selective circular dichroism^{3-7,26}. We point out that a (semi)metallic state appearing at the phase boundary between two topologically distinctive insulators is also protected topologically. We may call it a topological (semi)metal.

In what follows we use notations $s_z = \uparrow\downarrow$, $t_z = A, B$, $\eta = K, K'$ in indices while $s_z = \pm 1$, $t_z = \pm 1$, $\eta = \pm 1$ in equations for the spin, the sublattice pseudospin and the

valley, respectively. We also use the Pauli matrices σ_a and τ_a for the spin and the sublattice pseudospin, respectively.

II. HAMILTONIAN

Silicene is well described by the tight-binding model^{15,27},

$$H = -t \sum_{\langle i,j \rangle \alpha} c_{i\alpha}^\dagger c_{j\alpha} + i \frac{\lambda_{\text{SO}}}{3\sqrt{3}} \sum_{\langle\langle i,j \rangle\rangle \alpha \beta} \nu_{ij} c_{i\alpha}^\dagger \sigma_{\alpha\beta}^z c_{j\beta} - i \frac{2}{3} \lambda_{\text{R2}} \sum_{\langle\langle i,j \rangle\rangle \alpha \beta} t_z^i c_{i\alpha}^\dagger \left(\boldsymbol{\sigma} \times \hat{\mathbf{d}}_{ij} \right)_{\alpha\beta}^z c_{j\beta}, \quad (1)$$

where $c_{i\alpha}^\dagger$ creates an electron with spin polarization α at site i in a honeycomb lattice, and $\langle i, j \rangle / \langle\langle i, j \rangle\rangle$ run over all the nearest/next-nearest-neighbor hopping sites. The first term represents the usual nearest-neighbor hopping with the transfer energy $t = 1.6\text{eV}$. The second term represents the effective spin-orbit (SO) interaction with $\lambda_{\text{SO}} = 3.9\text{meV}$, and $\nu_{ij} = +1$ if the next-nearest-neighboring hopping is anticlockwise and $\nu_{ij} = -1$ if it is clockwise with respect to the positive z axis. The third term represents the Rashba interaction with $\lambda_{\text{R2}} = 0.7\text{meV}$, where $t_z^i = \pm 1$ for i representing the A (B) site; $\hat{\mathbf{d}}_{ij} = \mathbf{d}_{ij} / |\mathbf{d}_{ij}|$ with the vector \mathbf{d}_{ij} connecting two sites i and j in the same sublattice.

The low-energy effective Hamiltonian is given by the Dirac theory around the K_η point. The Hamiltonian (1) yields

$$H_\eta^0 = \hbar v_F (\eta k_x \tau_x + k_y \tau_y) + \lambda_{\text{SO}} \eta \tau_z \sigma_z + a \lambda_{\text{R2}} \eta \tau_z (k_y \sigma_x - k_x \sigma_y), \quad (2)$$

where $v_F = \frac{\sqrt{3}}{2} a t$ is the Fermi velocity with the lattice constant $a = 3.86\text{\AA}$.

A great merit of silicene is that we can introduce various potential terms into the Hamiltonian by making advantages of its bucked structure. There exist eight commuting terms which we are able to introduce into the Dirac Hamiltonian (2). They are

$$H_{pqr} = \lambda_{pqr} \eta^p (\sigma_z)^q (\tau_z)^r, \quad (3)$$

where $p, q, r = 0$ or 1 .

The coefficient of τ_z is the Dirac mass, to which four terms contribute. They are H_{pqr} with $r = 1$. First, H_{111} is nothing but the SO coupling term with $\lambda_{111} = \lambda_{\text{SO}}$. Second, H_{001} is the staggered sublattice potential term¹² with $\lambda_{001} = \ell E_z$, which is controlled by applying electric field E_z , where $\ell = 0.23\text{\AA}$ is the sublattice separation. Third, H_{101} is the Haldane term²⁸ with strength $\lambda_{101} = \lambda_\Omega$, which is controlled by applying photo-irradiation¹⁴. Finally, H_{011} is the new term we propose to analyze in the present work. As we see, it is the staggered exchange term with $\lambda_{011} = \Delta M$. We summarize the property of the Dirac mass term H_{pq1} with respect to the time-reversal symmetry (TRS), the spin-rotation symmetry (SRS) and the sublattice pseudospin symmetry (SLS)²⁹

as

H_{pq1}	potential term	TRS	SRS	SLS
111	Kane-Mele	true	false	false
001	s-sublattice	true	true	false
011	s-exchange	false	false	false
101	Haldane	false	true	false

(4)

where s- stands for staggered. We find that QAH effects can be induced by the Haldane term or the staggered exchange term since they break the TRS.

We address the other potential terms in (3), or H_{pqr} with $r = 0$. They induce the shift of Dirac cones and break the electron-hole symmetry, as we discuss in Section VI. First, H_{000} is nothing but the chemical potential with $\lambda_{000} = \mu$. Second, H_{010} is the mean exchange coupling term¹³ with $\lambda_{010} = \overline{M}$. The rest two terms H_{100} and H_{110} have not been discussed previously, and their experimental realizations would yet be explored. We may call H_{100} the staggered Haldane term with $\lambda_{100} = \lambda_{\text{SH}}$ and H_{110} the staggered Kane-Mele term with $\lambda_{110} = \lambda_{\text{SKM}}$. We summarize the symmetry property of the shift term H_{pq1} as

H_{pq0}	potential term	TRS	SRS	SLS
000	chemical potential	true	true	true
010	m-exchange	false	false	true
100	s-Haldane	false	true	true
110	s-Kane-Mele	true	false	true

(5)

where m- and s- stands for mean and staggered, respectively.

We may write down the tight-binding term that yields the potential term H_{pqr} . The additional terms are^{12,13}

$$\begin{aligned} \Delta H = & -\ell \sum_{i\alpha} t_z^i E_z c_{i\alpha}^\dagger c_{i\alpha} + i \frac{\lambda_\Omega}{3\sqrt{3}} \sum_{\langle\langle i,j \rangle\rangle \alpha \beta} \nu_{ij} c_{i\alpha}^\dagger c_{j\beta} \\ & + \sum_{i\alpha} M t_z^i c_{i\alpha}^\dagger \sigma_{\alpha\alpha}^z c_{i\alpha} + \mu \sum_{i\alpha} c_{i\alpha}^\dagger c_{i\alpha} \\ & + i \frac{\lambda_{\text{SH}}}{3\sqrt{3}} \sum_{\langle\langle i,j \rangle\rangle \alpha \beta} \tau_z \nu_{ij} c_{i\alpha}^\dagger c_{j\alpha} \\ & + i \frac{\lambda_{\text{SKM}}}{3\sqrt{3}} \sum_{\langle\langle i,j \rangle\rangle \alpha \beta} \tau_z \nu_{ij} c_{i\alpha}^\dagger \sigma_{\alpha\beta}^z c_{j\beta}. \end{aligned} \quad (6)$$

The Dirac Hamiltonian is

$$H_\eta = H_\eta^0 - \ell E_z \tau_z + \eta \lambda_\Omega \tau_z + \Delta M \sigma_z \tau_z + \mu + \overline{M} \sigma_z + \lambda_{\text{SH}} \eta + \lambda_{\text{SKM}} \eta \sigma_z, \quad (7)$$

where $\overline{M} = \frac{1}{2}(M_A + M_B)$ and $\Delta M = M_A - M_B$. The Dirac mass is given by

$$\Delta_{s_z}^\eta = \eta s_z \lambda_{\text{SO}} - \ell E_z + \eta \lambda_\Omega + s_z \Delta M, \quad (8)$$

which may be positive, negative or zero. We can make a full control of the Dirac mass independently for each spin and valley to materialize spin-valleytronics in silicene.

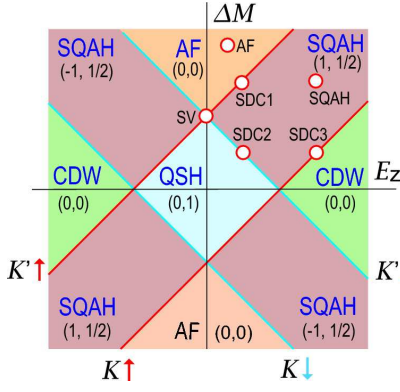


FIG. 1: (Color online) Phase diagram in the ℓE_z - ΔM plane. Heavy lines represent phase boundaries where the band gap closes. There are three types of topological insulators as indicated by QSH with $(0, 1)$ and SQAH with $(\pm 1, \frac{1}{2})$. There are two types of trivial band insulators as indicated by AF and CDW. There emerge the SDC semimetal and the SV semimetal in the phase boundary. A circle shows a point where the energy spectrum is shown in Fig.2. The gap closes at $E_z = \pm 17\text{meV}/\text{\AA}$ on the E_z axis and at $\Delta M = \pm \lambda_{\text{SO}}$ on the ΔM axis.

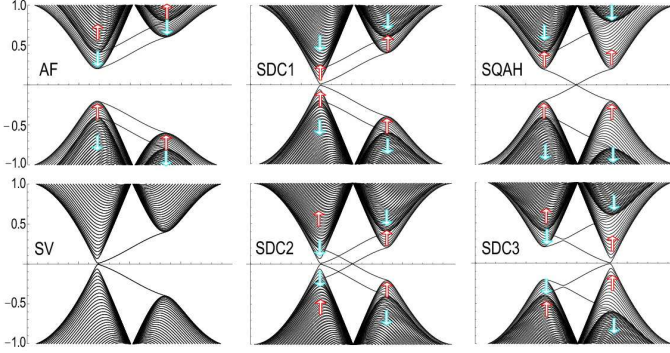


FIG. 2: (Color online) The band structures of zigzag silicene nanoribbons at the points indicated in the phase diagram [Fig.1]. The vertical axis is the energy in unit of t , and the horizontal axis is the momentum. We can clearly see the Dirac cones representing the energy spectrum of the bulk. Lines connecting the two Dirac cones are edge modes.

III. TOPOLOGICAL CHARGES

We first explore the Hamiltonian system with the mass correction terms H_{pq1} included. The Hamiltonian H_η is explicitly given by the 4×4 matrix as

$$H_\eta = \begin{pmatrix} H_\eta^\uparrow & R_\eta \\ R_\eta^\dagger & H_\eta^\downarrow \end{pmatrix}, \quad (9)$$

with the diagonal elements

$$H_\eta^{s_z} = \begin{pmatrix} \Delta_{s_z}^\eta & \hbar v_F(\eta k_x - i k_y) \\ \hbar v_F(\eta k_x + i k_y) & -\Delta_{s_z}^\eta \end{pmatrix}, \quad (10)$$

and the off-diagonal element

$$R_\eta = \begin{pmatrix} i a \lambda_{R2}(\eta k_x - i k_y) & 0 \\ 0 & -i a \lambda_{R2}(\eta k_x - i k_y) \end{pmatrix}. \quad (11)$$

Note that the off-diagonal element R_η vanishes at the K_η point where $k_x = k_y = 0$.

The characteristic feature is the existence of the electron-hole symmetry. The energy spectrum at the K_η point contains four levels, $\pm \Delta_{s_z}^\eta$, and the band gap is given by $2|\Delta_{s_z}^\eta|$. Topological phase transitions are controlled entirely by the spin-valley dependent Dirac mass $\Delta_{s_z}^\eta$.

We set $\lambda_{R2} = 0$ since it is a small quantity. We are able to justify this simplification in the present system, as we describe at the end of this section. When $\lambda_{R2} = 0$, the spin s_z is a good quantum number. The Dirac Hamiltonian is given by the 2×2 matrix $H_\eta^{s_z}$ for each spin s_z and each Dirac valley K_η . For such a system it is straightforward to calculate the spin-valley dependent Chern number $\mathcal{C}_{s_z}^\eta$ by integrating the Berry curvature over all occupied states of electrons in the momentum space. The Berry curvature is described by the meron configuration in the sublattice-pseudospin space, and the Chern number $\mathcal{C}_{s_z}^\eta$ becomes identical to the Pontryagin number³⁰. We find

$$\mathcal{C}_{s_z}^\eta = \frac{\eta}{2} \text{sgn}(\Delta_{s_z}^\eta) \quad (12)$$

as a function of the spin-valley dependent Dirac mass $\Delta_{s_z}^\eta$. This is well defined provided that the Fermi level is taken within the insulating gap. A phase transition may occur when one Dirac mass becomes zero, $\Delta_{s_z}^\eta = 0$ for certain η and s_z .

The topological quantum numbers are the Chern number \mathcal{C} and the spin-Chern number \mathcal{C}_s modulo 2. They are given by

$$\mathcal{C} = \mathcal{C}_\uparrow^K + \mathcal{C}_\uparrow^{K'} + \mathcal{C}_\downarrow^K + \mathcal{C}_\downarrow^{K'}, \quad (13a)$$

$$\mathcal{C}_s = \frac{1}{2} (\mathcal{C}_\uparrow^K + \mathcal{C}_\uparrow^{K'} - \mathcal{C}_\downarrow^K - \mathcal{C}_\downarrow^{K'}). \quad (13b)$$

We now switch on the Rashba interaction adiabatically, $\lambda_{R2} \neq 0$. As far as λ_{R2} is small, the band structure is almost unchanged. Furthermore, it follows from the Hamiltonian (9) that the phase transition point is independent of λ_{R2} and still given by solving $\Delta_{s_z}^\eta = 0$. Since the gap keeps open during this adiabatic process, the Chern numbers are well defined and their values are unchanged since they are quantized.

IV. PHASE DIAGRAM IN $(E_z, \Delta M)$ PLANE

For definiteness we investigate the topological phase transition in the $(E_z, \Delta M)$ plane, where

$$\Delta_{s_z}^\eta = \eta s_z \lambda_{\text{SO}} - \ell E_z + s_z \Delta M. \quad (14)$$

The phase boundaries are given by solving $\Delta_{s_z}^\eta = 0$, which yields four heavy lines corresponding to $s_z = \uparrow \downarrow$ and $\eta = K, K'$ in the phase diagram [Fig.1]. The spin-valley dependent Chern number $\mathcal{C}_{s_z}^\eta$ is calculated at each point $(E_z, \Delta M)$

with the use of (12), from which we derive the topological numbers $(\mathcal{C}, \mathcal{C}_s)$ based on (13). They take constant values in one phase, which we have depicted in the phase diagram. We illustrate the band structure of a nanoribbon with zigzag edges in Fig. 2, which manifests the spin-valley structure of topologically protected phases.

First, there appear four types of insulators:

- (1) The spin-polarized QAH (SQAH) insulators with $(\mathcal{C}, \mathcal{C}_s) = (\pm 1, \frac{1}{2})$.
- (2) The QSH insulator with $(0, 1)$.
- (3) The trivial charge-density-wave-type (CDW) band insulator with $(0, 0)$.
- (4) The trivial antiferromagnetic-order-type (AF) band insulator with $(0, 0)$.

We note that there are two types of trivial band insulators. The band gaps are different between the K and K' points in the AF insulator, while they are identical in the CDW insulator.

Second, SDC metals appear in the three phase boundaries of the SQAH insulator. The SDC metal is originally found in silicene by applying photo-irradiation and electric field simultaneously¹⁴. It is interesting that the SDC state is also obtainable without photo-irradiation. On the other hand, the SV semimetal appears at the point where the four topological insulators meet. They are topologically protected semimetals, since they appear in the interface of different topological insulators each of which is topologically protected against small perturbations.

V. INHOMOGENEOUS DIRAC MASS

We may apply an inhomogeneous electric field¹² $E_z(x, y)$ or generate a domain wall in the antiferromagnet $\Delta M(x, y)$, which makes the Dirac mass inhomogeneous. For simplicity we assume the homogeneity in the x direction. The zero modes appear along the line determined by $\Delta_{s_z}^\eta(y) = 0$, when $\Delta_{s_z}^\eta(y)$ changes the sign. We may set $k_x = \text{constant}$ due to the translational invariance along the x axis. We seek the zero-energy solution. The particle-hole symmetry guarantees the existence of zero-energy solutions satisfying the relation $\psi_B = i\xi\psi_A$ with $\xi = \pm 1$. Here, ψ_A is a two-component amplitude with the up spin and down spin. Setting $\psi_A(x, y) = e^{ik_x x} \phi_A(y)$, we obtain $H_\eta \psi_A(x, y) = E_{\eta\xi} \psi_A(x, y)$, together with a linear dispersion relation $E_{\eta\xi} = \eta\xi\hbar v_F k_x$. We can explicitly solve this as

$$\phi_{As_z}(y) = C \exp \left[\frac{\xi}{\hbar v_F} \int^y \Delta_{s_z}^\eta(y') dy' \right], \quad (15)$$

where C is the normalization constant. The sign ξ is determined so as to make the wave function finite in the limit $|y| \rightarrow \infty$. This is a reminiscence of the Jackiw-Rebbi mode³¹ presented for the chiral mode. The difference is the presence of the spin and valley indices in the wave function.

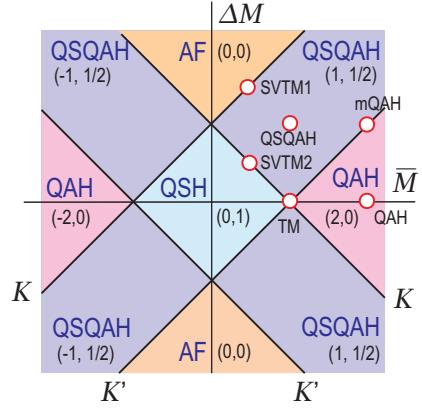


FIG. 3: (Color online) Phase diagram in the \overline{M} - ΔM plane. Heavy lines represent phase boundaries. There are five types of topological insulators as indicated by QAH with $(\pm 2, 0)$, QSQAH with $(\pm 1, 1/2)$ and QSH with $(0, 1)$. There is one trivial band insulator as indicated by AF. There emerge the mQAH metal and the TM in the phase boundary. A circle shows a point where the energy spectrum is calculated and shown in Fig. 4. The gap closes at $\overline{M} = \pm \lambda_{SO}$ on the \overline{M} axis and at $\Delta M = \pm \lambda_{SO}$ on the ΔM axis.

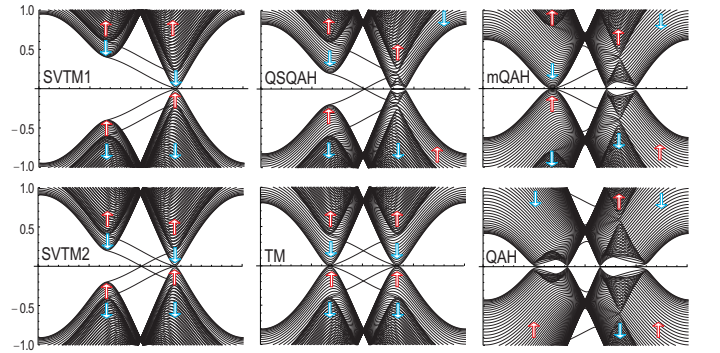


FIG. 4: (Color online) The band structures of silicene nanoribbons at marked points in the phase diagram [Fig. 3]. The vertical axis is the energy in unit of t , and the horizontal axis is the momentum. Lines connecting the two Dirac cones are edge modes.

VI. PHASE DIAGRAM IN $(\overline{M}, \Delta M)$ PLANE

We next investigate the Hamiltonian system by including the Dirac-cone shifting terms H_{pq0} . General analysis is quite difficult to make since there exists no electron-hole symmetry. For definiteness we only consider the mean-exchange-field term H_{010} . The Hamiltonian is given by (9) together with

$$H_\eta^{s_z} = \begin{pmatrix} \Delta_{s_z}^\eta + \overline{M}s_z & \hbar v_F(\eta k_x - i k_y) \\ \hbar v_F(\eta k_x + i k_y) & -\Delta_{s_z}^\eta + \overline{M}s_z \end{pmatrix}, \quad (16)$$

where the Dirac mass $\Delta_{s_z}^\eta$ is given by (8). The gap is no longer given solely by the Dirac mass.

The energy spectrum at the K_η point contains four levels, $\Delta_{s_z}^\eta + \overline{M}s_z$ and $-\Delta_{s_z}^\eta + \overline{M}s_z$ with $s_z = \pm 1$. The gap closes

at the K_η point when any two of them coincide,

$$\Delta_{s_z}^\eta = \pm \overline{M} s_z, \quad (17)$$

which in general gives the phase boundaries. However, the present analysis is not enough to construct the phase diagram, because the Dirac cones with the opposite spins touch one to another at the phase transition point. When they touch, the Rashba interaction ($\lambda_{R2} \neq 0$) mixes the up and down spins, yielding an essential modification of the band structure¹³. It is necessary to diagonalize the Hamiltonian (9) with the off-diagonal element (11) and the diagonal element (16).

Let us study explicitly the simplest case with the exchange fields M_A and M_B without any other external fields, where

$$\Delta_{s_z}^\eta = \eta s_z \lambda_{SO} + s_z \Delta M. \quad (18)$$

We give the phase diagram in the $(\overline{M}, \Delta M)$ plane [Fig.3]. The phase boundaries are given by solving (17), which yield four heavy lines corresponding to $s_z = \uparrow\downarrow$ and $\eta = K, K'$ in the phase diagram. We have four distinct regions referred to as QSH, AF, QAH and QSQA. We also illustrate the band structure of a silicene nanoribbon with zigzag edges [Fig.4] for typical points in the phase diagram.

When we set $\lambda_{R2} = 0$, only the QSH phase is an insulator. In all the other regions the conduction and valence bands penetrate into one another and are mixed.

When we include the Rashba interaction ($\lambda_{R2} \neq 0$), the collision is avoided since it turns the level crossing into the level anticrossing. Indeed, the energy spectrum consists of four levels,

$$E_{s_z}^\eta = \pm \sqrt{(a\lambda_{R2}k)^2 + F_\pm(k)^2}, \quad (19)$$

with $F_\pm(k) = \eta s_z \overline{M} \pm \sqrt{(\hbar v_F k)^2 + (\eta \lambda_{SO} + \Delta M)^2}$. We can see that the gap is open everywhere in the phase diagram except for the phase boundaries: Some typical examples of nanoribbon band structure are found in Fig.4.

Since the spin is no longer a good quantum number, the topological numbers are no longer given by the formulas (13). The Berry curvature is described by Skyrmions in the real spin space¹³. We are able to introduce the pseudospin-valley Chern number $C_{t_z}^\eta$ with $t_z = A, B$,

$$C_{t_z}^\eta = \frac{1}{2} \text{sgn}(\eta t_z \lambda_{SO} + M_{t_z}), \quad (20)$$

in terms of which the topological numbers are given by

$$\mathcal{C} = \mathcal{C}_A^K + \mathcal{C}_B^K + \mathcal{C}_A^{K'} + \mathcal{C}_B^{K'}, \quad (21a)$$

$$\mathcal{C}_s = \frac{1}{2} (\mathcal{C}_A^K - \mathcal{C}_B^K - \mathcal{C}_A^{K'} + \mathcal{C}_B^{K'}). \quad (21b)$$

They are calculated at each point (M_A, M_B) or $(\overline{M}, \Delta M)$. The topological numbers $(\mathcal{C}, \mathcal{C}_s)$ take constant values in one phase, which we have depicted in the phase diagram [Fig.3]. We illustrate the band structure of a nanoribbon with zigzag edges in Fig.4. Note that the spin becomes almost a good quantum number away from the K_η points.

First, there appear four types of insulators:

(1) The QSQA insulators with $(\mathcal{C}, \mathcal{C}_s) = (\pm 1, 1/2)$, where the QAH effect is realized at one valley in coexistence with the QSH effect at the other valley. It is intriguing that, e.g., the topological numbers $(\pm 1, 0)$ are assigned to the K point and $(0, 1/2)$ to the K' point.

(2) The trivial AF insulator with $(0, 0)$.

(3) The QSH insulator with $(0, 1)$.

(4) The QAH phases with $(2, 0)$ for $M > 0$ and $(-2, 0)$ for $M < 0$.

Second, at the boundary, the topological metal (TM) and the single-valley topological metal (SVTM) emerge. The band touches parabolically in them. Their emergencies are also protected topologically since they are sandwiched by different topological insulators.

VII. OPTICAL ABSORPTION

An interesting experiment to probe and manipulate the valley degree of freedom is optical absorption^{3-7,26}. We briefly discuss that spin-valley dependent band structures we have found will be experimentally observable by spin-valley-selective circular dichroism. Circular dichroism is a phenomena in which the response of the left- and right-handed circularly polarized light is different. To assess the optical selectivity of spin and valley by circularly polarized light, we compute the spin-valley dependent degree of circular polarization between the top valence bands and bottom of conduction bands. It is straightforward to apply the standard method^{3-7,26} to calculate an optical absorption.

We consider the interband matrix elements of the left- and right-polarized radiation fields (\pm) for spin s_z at k for a vertical transition from band u_c to band u_v . They are defined by

$$P_\pm^\eta(k) \equiv m_0 \langle u_c(k) | \frac{1}{\hbar} \frac{\partial H_\eta}{\partial k_\pm} | u_v(k) \rangle. \quad (22)$$

If we neglect the Rashba terms ($\lambda_{R2} = 0$), we are able to obtain an analytic formula for the transitions near the K_η point as

$$|P_\pm^\eta(k)|^2 = m_0^2 v_F^2 \left(1 \pm \eta \frac{\Delta_{s_z}^\eta}{\sqrt{(\Delta_{s_z}^\eta)^2 + 4a^2 t^2 k^2}} \right)^2. \quad (23)$$

Especially we find the spin-valley dependent optical selection rule at $k = 0$,

$$|P_\pm^\eta(0)|^2 = m_0^2 v_F^2 [1 \pm \eta \text{sgn}(\Delta_{s_z}^\eta)]^2, \quad (24)$$

which will be detected experimentally. Such a spin-valley selective circular dichroism would lead to the eventual realization of spin-valleytronics.

VIII. DISCUSSION

In this paper, exploiting advantages of the buckled structure, we have proposed to make a full control of the Dirac

mass and hence a full control of the topological charges in silicene. A topological state has a particular spin-valley structure. In exploring the phase diagram, we have found a hybrid topological insulator named Quantum-Spin-Quantum-Anomalous Hall (QSQA) insulator, where two different topological insulators coexist: The QSH effect is realized at one valley while the QAH effect is realized at the other valley. The topological numbers are simply given by one half of the sum of those of the QSH and QAH insulators. Such a hybrid of two distinctive topological insulators is utterly a new state.

We address a question how realistic it is to generate various topological insulators such as the QSQA state. In order to make the QSQA phase, the exchange interaction at the A (B) site should be larger (smaller) than the SO interaction, whose magnitude is 3.9meV. When we attach a ferromagnet to the side of A sites, the exchange field at B sites is naturally

smaller than that at A sites. Since the magnitude of the exchange field induced by transition metal deposition is of the same order of the SO interaction¹⁷, it is plausible that the condition for the QSQA phase can be satisfied in a realistic experimental situation. Furthermore, we can think of three possible methods to produce exchange fields acting separately on the A and B sublattices. First, we sandwich silicene by two different ferromagnets. Second, we arrange two different transition metals so as to be absorbed as adatoms separately to the A and B sublattices. Third, we attach a honeycomb-lattice antiferromagnet⁷ or ferrimagnet to silicene. What kind of materials one should use will be a future problem.

I am very much grateful to N. Nagaosa for many fruitful discussions on the subject. This work was supported in part by Grants-in-Aid for Scientific Research from the Ministry of Education, Science, Sports and Culture No. 22740196.

-
- ¹ A. Rycerz, J. Tworzydło, and C. W. J. Beenakker, *Nat. Phys.* **3**, 172 (2007).
 - ² D. Xiao, W. Yao, and Q. Niu, *Phys. Rev. Lett.* **99**, 236809 (2007).
 - ³ W. Yao, D. Xiao, and Q. Niu, *Phys. Rev. B* **77**, 235406 (2008).
 - ⁴ D. Xiao, G.-B. Liu, W. Feng, X. Xu, and W. Yao, *Phys. Rev. Lett.* **108**, 196802 (2012).
 - ⁵ H. Zeng, J. Dai, W. Yao, D. Xiao and X. Cui, *Nat. Nanotech.* **7**, 490 (2012).
 - ⁶ T. Cao, G. Wang, W. Han, H. Ye, C. Zhu, J. Shi, Q. Niu, P. Tan, E. Wang, B. Liu and J. Feng *Nat. Com.* **3**, 887 (2012).
 - ⁷ X. Li, T. Cao, Q. Niu, J. Shi, and J. Feng, *cond-mat/arXiv:1210.4623*
 - ⁸ P. Vogt, P. De Padova, C. Quaresima, J. A., E. Frantzeskakis, M. C. Asensio, A. Resta, B. Ealet and G. L. Lay, *Phys. Rev. Lett.* **108**, 155501 (2012).
 - ⁹ A. Fleurence, R. Friedlein, T. Ozaki, H. Kawai, Y. Wang, and Y. Yamada-Takamura, *Phys. Rev. Lett.* **108**, 245501 (2012).
 - ¹⁰ C.-L. Lin, R. Arafune, K. Kawahara, N. Tsukahara, E. Minamitani, Y. Kim, N. Takagi, M. Kawai, *Appl. Phys. Express* **5**, 045802 (2012).
 - ¹¹ C.-C. Liu, W. Feng, and Y. Yao, *Phys. Rev. Lett.* **107**, 076802 (2011).
 - ¹² M. Ezawa, *New J. Phys.* **14**, 033003 (2012).
 - ¹³ M. Ezawa, *Phys. Rev. Lett.* **109**, 055502 (2012).
 - ¹⁴ M. Ezawa, *Phys. Rev. Lett.* **110**, 026603 (2013).
 - ¹⁵ C. L. Kane and E. J. Mele, *Phys. Rev. Lett.* **95**, 226801 (2005).
 - ¹⁶ M. Onoda and N. Nagaosa, *Phys. Rev. Lett.* **90**, 206601 (2003).
 - ¹⁷ Z. Qiao, S. A. Yang, W. Feng, W.-K. Tse, J. Ding, Y. Yao, J. Wang, and Q. Niu, *Phys. Rev. B* **82**, 161414 R (2010).
 - ¹⁸ W.-K. Tse, Z. Qiao, Y. Yao, A. H. MacDonald, and Q. Niu, *Phys. Rev. B* **83**, 155447 (2011).
 - ¹⁹ J. Ding, Z. Qiao, W. Feng, Y. Yao and Q. Niu, *Phys. Rev. B* **84**, 195444 (2011).
 - ²⁰ Z. Qiao, H. Jiang, X. Li, Y. Yao and Q. Niu, *Phys. Rev. B* **85**, 115439 (2012).
 - ²¹ C.-X. Liu, X.-L. Qi, X. Dai, Z. Fang and S.-C. Zhang, *Phys. Rev. Lett.* **101**, 146802 (2008).
 - ²² M.Z. Hasan and C. Kane, *Rev. Mod. Phys.* **82**, 3045 (2010).
 - ²³ X.-L. Qi and S.-C. Zhang, *Rev. Mod. Phys.* **83**, 1057 (2011).
 - ²⁴ C. Wu, B.A. Bernevig and S.-C. Zhang, *Phys. Rev. Lett.* **96**, 106401 (2006).
 - ²⁵ H. B. Nielsen and M. Ninomiya, *Nucl. Phys. B* **185**, 20 (1981).
 - ²⁶ M. Ezawa, *Phys. Rev. B* **86**, 161407(R) (2012).
 - ²⁷ C.-C. Liu, H. Jiang, and Y. Yao, *Phys. Rev. B*, **84**, 195430 (2011).
 - ²⁸ F. D. M. Haldane, *Phys. Rev. Lett.* **61**, 2015 (1988).
 - ²⁹ S. Ryu, C. Mudry, C.Y. Hou and C. Chamon, *Phys. Rev. B* **80**, 205319 (2009).
 - ³⁰ M. Ezawa, *Eur. Phys. J. B* **85**, 363 (2012).
 - ³¹ R. Jackiw and C. Rebbi, *Phys. Rev. D* **13**, 3398 (1976).